# Phase Separation and Mechanical Properties of Polyketone/Polyamide Polymer Alloys

**Atsushi Kato,[1] Maiko Nishioka,[1] Youhei Takahashi,[1] Toshiya Suda,[1] Hisahiro Sawabe,[1] Ayano Isoda,[1] Olga Drozdova,[1] Toshinori Hasegawa,[1] Toshihiro Izumi,[1] Kazuya Nagata,[2] Shigeki Hikasa,[3] Hitoshi Iwabuki,[3] Atsushi Asano[4]**

[1]*Research Department, Nissan Arc, Ltd., 1, Natsushima-cho, Yokosuka, Kanagawa 237-0061, Japan*
[2]*Department of Advanced Technology Development, Laboratory of Plastics, Asahikasei Chemicals Corporation, 1-3-1 Yakoh, Kawasaki-ku, Kawasaki, Kanagawa 210-0863, Japan*
[3]*Industrial Technology Center of Okayama Prefecture, 5301 Haga, Okayama 701-1296, Japan*
[4]*Department of Applied Chemistry, National Defense Academy, 1-10-20 Hashirimizu, Yokosuka, Kanagawa 239-8686, Japan*

Received 6 November 2008; accepted 8 November 2009
DOI 10.1002/app.31850
Published online 12 February 2010 in Wiley InterScience (www.interscience.wiley.com).

**ABSTRACT:** We have investigated polyketone (PK)/polyamide 6 (PA) polymer alloys having enhanced Charpy impact energy greater than that of polycarbonate (PC) as a result of moisture absorption. From the results of differential scanning calorimetry (DSC), Raman spectroscopy, and transmission electron microscope (TEM) observation of the polymer alloys, it was found that PK-rich and PA-rich phases exist at the nanometer level in the polymer alloys; however, a microscopic interaction phase formed between the two phases. 3D-TEM observations, electron energy loss spectroscopy, and small-angle X-ray scattering measurements revealed that a co-continuous nanolayer formed from the PA-rich phase and lamella network of the PK-rich phase. Moreover, the interaction and mobility of PK and PA molecular chains were investigated by using a $^{13}C$ cross polarization/magic angle sample spinning NMR technique. It was found that moisture absorption markedly enhances the mobility of PA molecular chains in PK/PA alloys. This suggests that the wet (moisture-absorbed) PA phase of PK/PA alloys allows quick deformation upon impact stimulation. On the other hand, the results of Charpy impact tests showed that the total impact energy ($E_{total}$) of the wet polymer alloy was much higher than that of the dry one. An examination of the load-displacement curves revealed that the wet samples showed a pronounced increase in displacement compared with the dry ones. From these results, it was concluded that the lamella network of the PK-rich phase sustains the maximum stress and that the large displacement of the PA-rich phase increases the impact energy. © 2010 Wiley Periodicals, Inc. J Appl Polym Sci 116: 3056–3069, 2010

**Key words:** alloys; morphology; phase separation; lamellar; impact resistance

## INTRODUCTION

There are strong desires for the development of impact-resistant plastic materials for the application to various auto parts to improve the safety of vehicles. Potential applications include plastic bumpers, outer body panels, door handles, trim parts, fenders, wheel caps, and various types of shock-absorbing parts.[1–4] The plastic bodies of cameras, video cameras, and mobile phones also require strong impact resistance to protect internal optical and electronic parts from damage when such devices are dropped or subjected to severe impacts.[5] Impact-resistant plastics that have been developed for such applications include polycarbonate (PC), high-impact polystyrene (HIPS), polypropylene (PP) copolymers, and polymer blends or alloys made of these polymers, as well as composites and other materials.[6–13]

Several mechanisms have been reported so far concerning the impact resistance of polymeric materials. According to Kuriyama,[14] the mechanisms manifesting impact resistance in polymers that have been examined in recent years include the formation of crazes or cavitation, shear (yield) deformation, and absorption of impact energy by the fracturing of the adhesive interface between the matrix and the disperse phase. Wu[6] and Yamamoto and Furukawa[8] described a mechanism for impact energy absorption by the formation of crazes, representing a structure characteristic of polymeric materials. Among other materials, such crazes have been observed in PC and in rubber-modified HIPS and ABS. It will be noted that the whitening of the deformed or impacted part

*Correspondence to:* A. Kato (kato@nissan-arc.co.jp).

of typical rubber-reinforced plastics such as ABS and HIPS is the result of the scattering of fine light due to cavitation, crazing, micro crack, etc. Especially for such ABS materials that are characterized by high rubber volume fraction whitening has been often observed only as a result of rubber cavitation. Bucknall[15] reported that stress concentrations near cavitated rubber particles promote multiple crazing for rubber-modified HIPS. The energy dissipation due to the generation and termination of these multiple crazes by rubber particles results in the high impact energy absorption of HIPS. According to Bucknall,[16] EPR was added to PP matrix and a weak part was introduced to the matrix. As a result, the cavitation was positively occurred in this blend and the toughness was improved. He pointed out that in order to understand the crazing and cavitation processes in the study and development of materials is very important for both the intrinsic understanding of the mechanisms of the deformation and for many industrial applications. The possibility of maximizing the energy absorbed by a polymer before failure occurs is connected to the creation of more surface area in the body of the polymer through crazing and cavitation processes. In addition, Narisawa[17] and Fu and Shen[18] demonstrated that impact resistance was improved by craze formation induced by the filler. Nagata et al.[19] also reported that impact resistance was markedly improved by the formation of many crazes in PP blended with a hybrid filler consisting of talc and calcium carbonate.

Further, it has also been reported that shear yielding or plastic deformation and craze formation increase impact strength. Elastomeric inclusions in thermoplastic matrices have been studied extensively in recent years. The primary role of rubber particles is to relieve stress triaxiality at the crack tip through internal cavitations, thereby promoting toughening mechanisms such as shear deformation in the matrix ligament.[15,16] Okamoto et al.[20] showed that the impact resistance of HIPS originated in plastic deformation and craze formation, and Cleslinski et al.[21] showed on the basis of their transmission electron microscope (TEM) observations of impact-resistant PP that shear yield deformation at room temperature and craze formation below the ductile-brittle transition point increased impact strength. Chakrabarty et al.[22] reported that the fracture mechanism in an epoxy resin/poly(ethyl methacrylate) interpenetrating polymer network changes from shear to craze formation accompanying an increase in the content of poly(ethyl methacrylate). The work done by Pecorini and Calvert[23] has made it clear that reactive ethylene/methyl acrylate/glycidyl methacrylate ternary copolymer/PET with dispersed particles smaller than 200 nm shows super-toughness due to the massive shear yielding of the matrix, whereas with dispersed particles larger than 200 nm, it exhibits super-toughness due to multiple crazing of the matrix. With regard to the improvement of impact resistance due to cavitation or microvoid formation, Hobbs et al.[24] reported that a combination of cavitation and shear deformation absorbed impact energy in a polyester/(bisphenol A) PC polymer alloy. Kim and Michler[25] suggested that cavitation in the stretched rubber shell and in the rubber particles as well as microvoid formation due to interfacial debonding between the particles and the matrix contributed to increased impact resistance in PP and PA66 dispersed with rubber particles. Bucknall[15] reported that deformation of the rubber phase and the formation of cavitation within the rubber phase improved impact resistance in EPR-blended PP. Additionally, Bucknall and Gilbert[26] reported that when PEI was added to epoxy resin, the phase-inversed structure where PEI was assumed to be a continuous phase was formed, and that epoxy resin was made tough as the ductile fracture of the PEI continuous phase occurred when destroying it.

It has also been pointed out that interfacial adhesion between different types of polymers is important in impact-resistant polymer alloys. Phan et al.[27] reported that improvement of interfacial adhesion between PP and rubber in a maleated PP/maleated natural rubber blend increased fracture toughness, impact strength, and rate of elongation. Chen et al.[28] showed that improvement of adhesion at the phase separation boundary improved impact strength in an ethylene-α-olefin copolymer rubber and maleated derivative/PA blend.

Meanwhile, Nagata et al.[29] have recently reported that a polymer alloy of ethylene/propylene/carbon monoxide (polyketone, PK) and polyamide 6 (PA) exhibited stiffness equal to or greater than PC and higher Izod impact strength greater than 0.05 to 1 kJ/m of PC.[30,31] Surprisingly, they found that the absorption of moisture markedly improved the impact strength of this alloy. Nagata et al.[29] also performed scanning electron microscope (SEM) and TEM observations of this alloy and reported that a PA-rich phase was dispersed in the PK matrix as an island phase of 100–200 nm in size. Furthermore, their measurements of viscoelasticity revealed that the loss tangent (tan δ) exhibited singular behavior and shifted to the low temperature side due to increased absorption of moisture.[29] These results imply that improvement of Izod impact strength is related to the phase separation structure of PK and PA, and that the absorption of moisture markedly promotes such improvement.

Therefore, in this study, the interaction of PA and PK in the polymer alloy was evaluated by Raman spectroscopy. The phase separation and higher-order structure were observed by using a TEM and a 3D-

**TABLE I**
**Weight Ratio of PK/PA Polymer Alloys**

| Samples | Ingredient (mass %) | |
|---|---|---|
| | PK[a] | PA[b] |
| K100 | 100 | 0 |
| K90A10 | 90 | 10 |
| K80A20 | 80 | 20 |
| K70A30 | 70 | 30 |
| K60A40 | 60 | 40 |
| K50A50 | 50 | 50 |
| K40A60 | 40 | 60 |
| K30A70 | 30 | 70 |
| K20A80 | 20 | 80 |
| K10A90 | 10 | 90 |
| K100 | 0 | 100 |

[a] Polyketone (ethylene/propylene/CO copolymer).
[b] Polyamide 6.

TEM. The dispersion of nitrogen originating from PA was detected by electron energy loss spectroscopy (EELS). Furthermore, the lamella network structure and molecular motion of the PK/PA polymer alloys were investigated by small-angle X-ray scattering (SAXS) measurement and a solid-state high resolution nuclear magnetic resonance (NMR) technique. In addition, in order to examine the impact fracture mechanism of the polymer alloy, the instrument Charpy impact testing was used this time. The macroscopic mechanism involved in the improvement of impact resistance due to the absorption of moisture was examined based on the load-displacement behavior, crack generation energy, and crack propagation energy measured for dry and wet polymer alloy test samples with an instrumented Charpy impact testing machine. The relationship between the aforementioned morphology and impact properties is discussed below based on the results.

## EXPERIMENTAL

### Material

The polymer alloys examined in this study consisted of an ethylene/propylene/CO copolymer (Carilon D26HM100, Shell Co.), i.e., PK and PA 6 (Amilan CM1017, Toray Ind.). Table I shows the mixing ratios of the polymer alloys used. From the left-hand side, the table shows the name of each sample and the mixing ratio of each polymer. For example, the sample indicated as K60A40 was blended of 60 mass % of PK (volume fraction 0.578) and 40 mass % of PA (volume fraction 0.422) by mechanical mixing using an twin-screw extruder (TEX-30α, Japan Steel Works) at 235°C. Polymer alloy impact test specimens (unnotched) were then molded at a resin temperature of 245°C and a mold temperature of 70°C using an injection molding machine (J50E II, Japan Steel Works).

Wet test specimens were then moisture-conditioned by holding them at 50% RH and a temperature of 23°C for 3 weeks. Dry test specimens were prepared by drying them in a vacuum at 100°C for 72 h. The moisture absorption rate of the test specimens was determined by measuring their water content with the Karl Fisher method. The test specimens were then hermetically sealed in aluminum foil laminated bags and stored in a refrigerator until just before the Charpy impact test. To avoid any change in the notch shape due to moisture conditioning or drying, a Type A notch (opening angle: 45° ± 1°; notch radius: 0.25 mm ± 0.05 mm; depth: 2.0 mm ± 0.1 mm) was machined to prepare notched test specimens just before the impact test. The size of the specimens used in the instrumented Charpy impact tests is shown in Figure 1. This test specimen size conforms to Japanese Industrial Standard (JIS) K7111, "Testing method for determining Charpy impact strength of plastics."

## APPARATUS AND PROCEDURE

### Differential scanning calorimetry

Differential scanning calorimetry (DSC) was performed with a TA instrument DSC-Q100 equipment. The sample was heated from 0°C to 80°C at a scan rate of 10°C/min in nitrogen gas atmosphere. The stepwise change of heat flow corresponds to the glass transition temperature ($T_g$).

### Raman spectroscopy

A microtome was used to cut thin slices parallel to the flow direction of the molten resin from the area of the impact test specimens where the thickness had been reduced by one-half. A microscope Raman spectrometer (SENTERRA TM, Bruker Optics Co.) was used to measure the Raman shift of the C=O functional group (1709 $cm^{-1}$) of PK and the

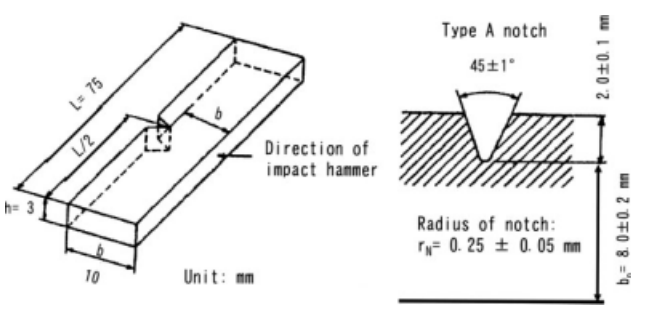


**Figure 1** Size of samples used in instrumented Charpy impact test.

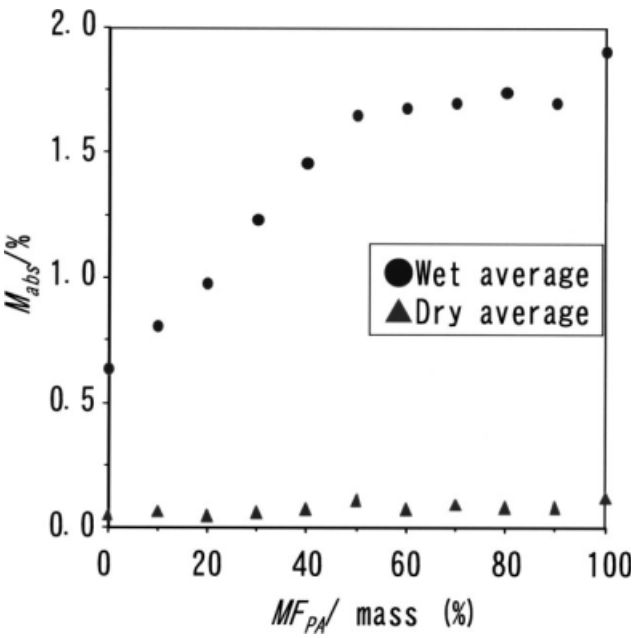


**Figure 2** Moisture absorption rate ($M_{abs}$) of PK/PA polymer alloy samples as a function of PA mass fraction ($MF_{PA}$). Moisture absorption condition in 50% RH at 23°C for 3 weeks. Drying condition in a vacuum at 100°C for 72 h. Measurement of moisture absorption, $M_{ads}$, of the polymer alloy was measured by the Karl Fisher method.

NHC=O functional group (1638 $cm^{-1}$) of PA in these thin samples when illuminated with a 5-μm-diameter beam at an excitation light wavelength of 785 nm.

### SEM observation

Platinum was first vapor-deposited on the Charpy impact fracture surface, which was then observed using a Hitachi S-4700 SEM at an accelerating voltage of 15 kV.

### TEM and 3D-TEM observation

An ultra-microtome was used to cut thin samples from the PK/PA polymer alloys that were frozen at the temperature of liquid nitrogen (−198°C). A pretreatment process called the NISSAN ARC-SG method[32,33] was then applied to make the thickness of the thin samples uniform and to smooth their surface simultaneously. The size of the samples thus obtained for 3D-TEM observation was approximately 500 nm in length, 500 nm in width, and 200 nm in thickness, and they were subjected to TEM and 3D-TEM observations with phosphotungstic acid staining.

The instruments used in the TEM and the 3D-TEM observations were a H-800 TEM (Hitachi) and a Tecnai G2 F20 TEM (FEI Co.), with the accelerating voltage of the electron beam set at 200 kV. In the 3D-TEM observation, samples were tilted in a tilting angle range from −70° to +70°, and image data (tilted images) were sequentially obtained at angle steps of 2°. Specifically, a sequential series of 71 tilted images in total were automatically input into the computer.[32,33] Using the IMOD program (software developed at the University of Colorado)[34] installed on the Tecnai TEM, the sequential tilted images were then converted to image slices showing the mass density distribution at each angle. The AMIRA program (developed by TGS Co.)[35] was then used to reconstruct 3D images from the image slices. In addition, a mapping image of N in the polymer alloys was also carried out by EELS using the Tecnai G2 F20.

### SAXS measurement

The long period of the lamella of the PK/PA polymer alloys was estimated using a SAXS instrument (Nano-STAR provided by Bruker AXS K. K.). A Cu Kα X-ray source and a two-dimensional detection machine were used for this purpose. The distance between the sample and the detector (camera length) was 106 cm.

### Solid-state high resolution NMR measurement

The molecular motions of PK and PA in the PK/PA polymer alloys were measured by a solid-state high resolution NMR (Varian NMR Systems 400WB, Varian). The $^{13}C$ cross polarization (CP)/magic angle sample spinning (MAS) NMR method was used. Cut samples of several mm in size were placed in the NMR sample tube having a diameter of 5 μm. The samples were measured at an observation frequency of 100.7 MHz and a MAS speed 6 kHz.

### Instrumented Charpy impact test

Instrumented Charpy impact tests were conducted according to the procedure specified in JIS K7111 at a temperature of approximately 24°C and at about 45% RH. The impact tester used was a CHARPAC-FRII (Yonekura MFG Co.) and the data obtained were analyzed using the IITMWin19 software (Yonekura MFG Co.) designed for processing Charpy impact test data. The results obtained from the analysis were load-displacement curves, crack generation energy, crack propagation energy, and the total impact absorption energy.

## RESULTS AND DISCUSSION

### Relationship between moisture absorption rate and PA volume fraction

The moisture absorption rate ($M_{abs}$) of the PK/PA polymer alloy samples is shown in Figure 2 as a

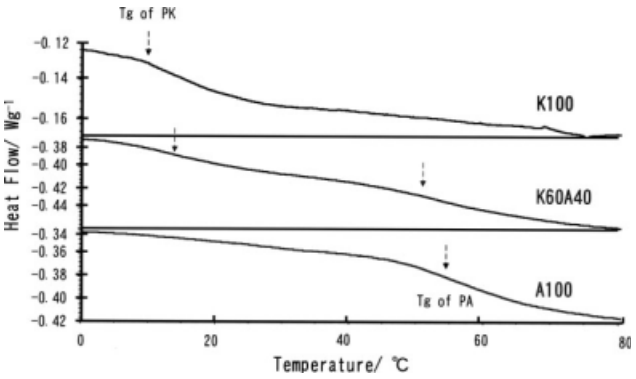


**Figure 3** DSC thermograms of dry K100, A100, and K60A40.

function of the PA mass fraction ($MF_{PA}$). For the wet samples, $M_{abs}$ increases linearly with $MF_{PA}$ only in the range 0 mass % $\leq MF_{PA} \leq$ 50 mass % and is approximately constant for higher $MF_{PA}$ values. For the dry samples, $M_{abs}$ seems to be almost constant with very small values. The larger difference between the wet and dry samples suggests that $M_{abs}$ was not simply dependent on $MF_{PA}$. On the other hand, $M_{abs}$ remained almost constant in the region of 50 mass % $\leq MF_{PA} \leq$ 100 mass %. These results imply that this behavior may be dependent on the phase separation of the PK/PA polymer alloys.

### Glass transition temperature of polymer alloy

Feng and Chan[36] reported that the glass transition temperature ($T_g$) of poly(methyl methacrylate) (PMMA) in the blends of an alternating ethylene-tetrafluorethylene copolymer (ETFE) moves to low temperatures when the ETFE content increases. They thought that this result confirms that only weak interactions exist between ETFE and PMMA. In this study, the $T_g$'s of the component polymers (dry PK and PA) and their polymer alloy (dry K60A40) was examined. Figure 3 shows the DSC thermograms of dry K100, A100, and K60A40. The thermograms of PK and PA show two distinguishable $T_g$ values (ca. 10°C and ca. 55°C, respectively) corresponding to the respective neat polymers, whereas K60A40 has two $T_g$'s (ca. 14°C and ca. 51°C) and they are located between the $T_g$ of PK and that of PA. This result suggests that an interaction between PK and PA components occurs in K60A40, and this is supported by the below-mentioned result of the measurement of the Raman spectroscopy.

### Interaction between PK and PA

Figure 4 shows the Raman spectra of each PK/PA polymer alloy sample. The peak intensity of the NHC=O functional group (1638 $cm^{-1}$) increased with a larger PA volume fraction. Similarly, the peak intensity of the C=O functional group (1709 $cm^{-1}$) increased with a larger PK volume fraction. Additionally, the peak of the C=O functional group tended to shift slightly toward the low frequency side with an increase in the PA volume fraction. This tendency presumably reflects the interaction between the PK and PA phases.

The change in the composition of the PK/PA polymer alloys was then evaluated using the peak intensity ratio of the Raman spectra. The spectra of the C=O functional group (1709 $cm^{-1}$) of PK and the NHC=O functional group (1638 $cm^{-1}$) of PA are diagramed schematically in Figure 5(a). The peak intensity ($I_{PK}$, $I_{PA}$) was defined as the height from the baseline at the bottom of each peak to the top of the peak, and the peak intensity ratio of PA and PK was defined as $I_{PA}/I_{PK}$. Because $I_{PA}$ and $I_{PK}$ reflect the content of each constituent polymer, the relationships between the peak intensities and volume fractions can be expressed as shown in eqs. (1)–(3).

$$\phi_{PA} + \phi_{PK} = 1 \tag{1}$$

where $\phi_{PA}$ and $\phi_{PK}$ are the volume fraction of PA and PK, respectively.

$$\phi_{PA} = \alpha I_{PA} \tag{2}$$

where $\phi_{PA}$ is a coefficient for converting the peak intensity of PA to the volume fraction.

$$\phi_{PK} = \beta I_{PK} \tag{3}$$

where $\phi_{PK}$ is a coefficient for converting the peak intensity of PK to the volume fraction.

Substituting eqs. (2) and (3) into eq. (1) and arranging the expression yields eq. (4).

$$I_{PA} \Big/ I_{PK} = \left(\beta \Big/ \alpha\right)\left[\frac{\phi_{PA}}{1 - \phi_{PA}}\right] \tag{4}$$

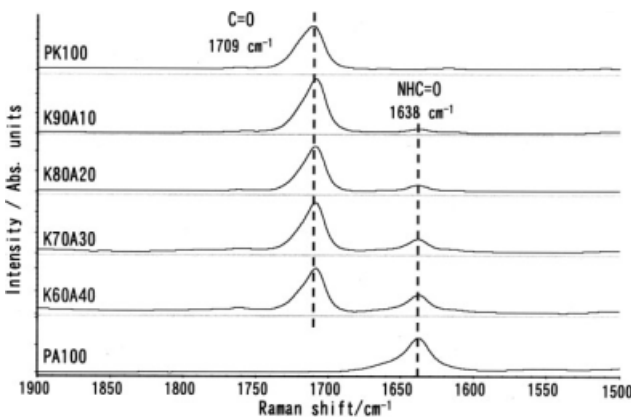


**Figure 4** Raman spectra of PK/PA polymer alloys.

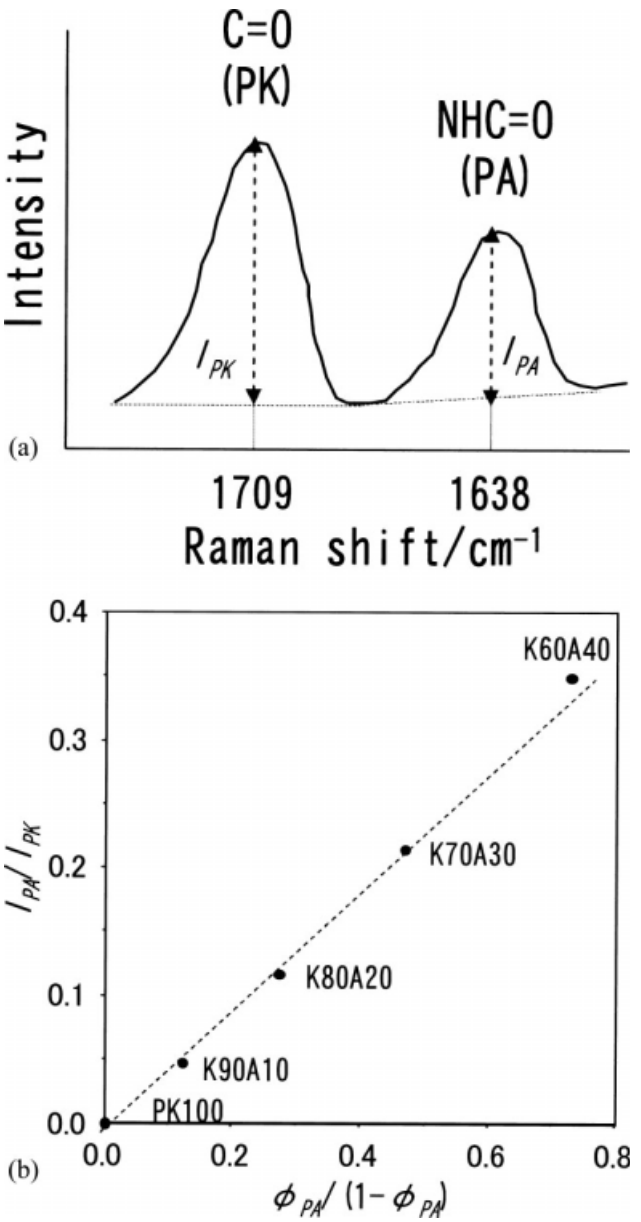


**Figure 5** Relationship between intensity ratio ($I_{PA}/I_{PK}$) of Raman peak and function of PA volume fraction ($\phi_{PA}/(1 - \phi_{PA})$). (a) Schematic diagram of peak intensity of Raman shift. $I_{PK}$: Intensity of PK. $I_{PA}$: Intensity of PA. (b) Relationship between ($I_{PA}/I_{PK}$) and ($\phi_{PA}/(1 - \phi_{PA})$. Linear approximation equation. $I_{PA}/I_{PK} = 0.48\phi_{PA}/(1 - \phi_{PA})$. Variance ($R^2$) = 0.998.

It is clear from eq. (4) that $I_{PA}/I_{PK}$ and $\phi_{PA}/(1 - \phi_{PA})$ are directly proportional if the composition of PA and PK does not change due to the bonding environment. The relationship between $I_{PA}/I_{PK}$ and $\phi_{PA}/(1 - \phi_{PA})$ is shown in Figure 5(b). A good direct proportional relationship between the two is seen for all the polymer alloy samples used in this study. This indicates that PA and PK were physically mixed in all the polymer alloys and that no chemical reactions (i.e., thermal decomposition and degradation, oxidation, hydrolysis, polymer reaction, and copolymerization, etc.) occurred between them because PK and PA are thermally and chemically stable under this mixing and molding conditions. That is, the temperatures of the thermal oxidative decomposition of PK and PA are 320°C[37] and 408°C,[38] respectively. PK is not oxidized easily and does not form the carboxyl compounds which can react with PA.[37]

To investigate the interaction between the PK and PA phases, the full width at half maximum (FWHM) of the Raman shift peak was defined as shown in

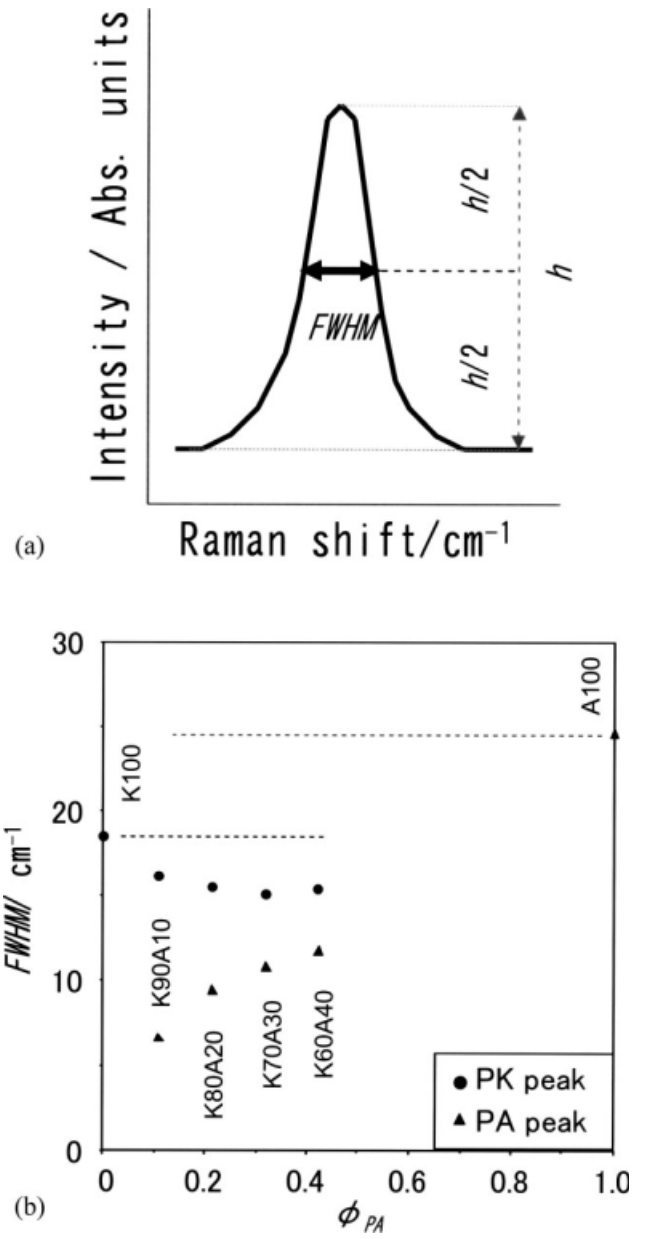


**Figure 6** Analysis results of full width at half maximum (*FWHM*) of Raman spectra of PK/PA polymer alloys. (a) Schematic diagram of Raman shift peak. *h*: Height of Raman peak. *FWHM*: Width of the peak at *h*/2. (b) Dependence of FWHM of Raman shift peaks on volume fraction ($\phi_{PA}$) of PA.

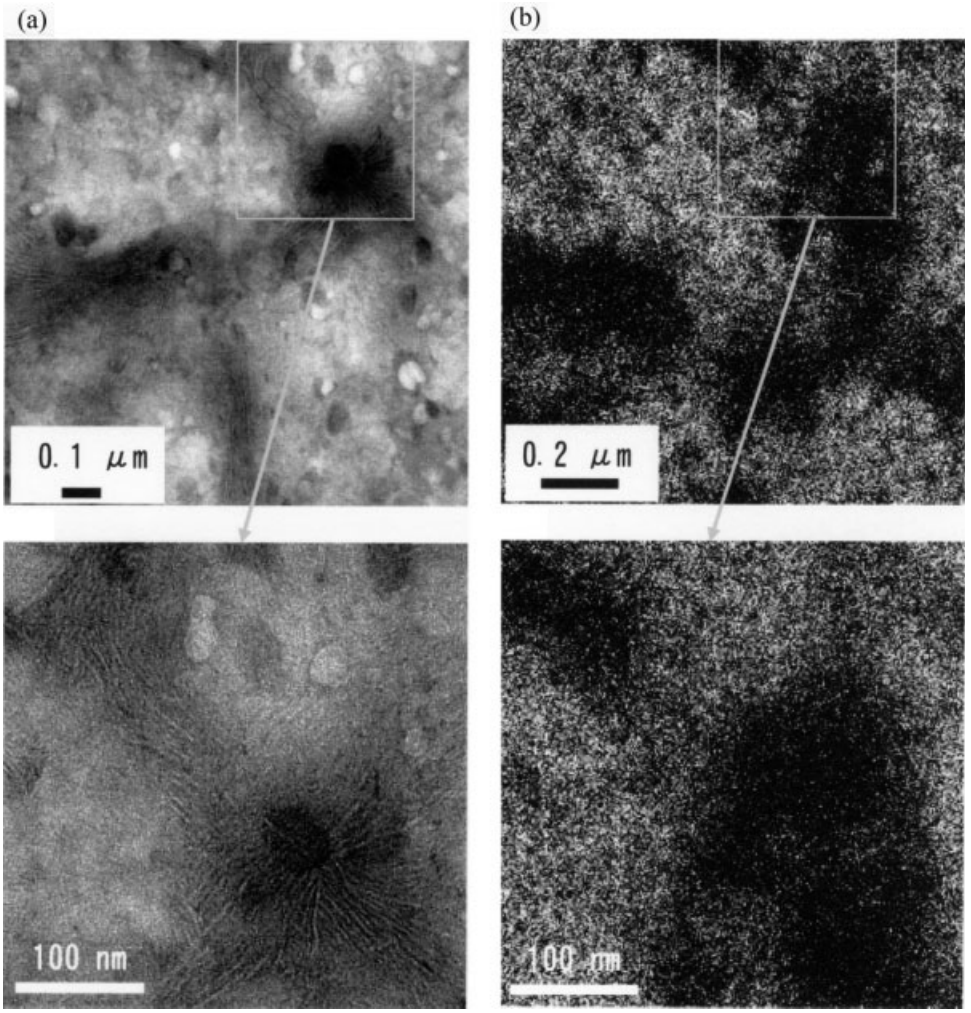


**Figure 7** TEM and EELS (electron energy loss spectroscopy) images of K60A40: (a) TEM images, (b) EELS images.

Figure 6(a). The relationship between *FWHM* and $\phi_{PA}$ is shown in Figure 6(b). The closed circles and closed triangles in the figure show the measured *FWHM* values for the PK and PA peaks, respectively. It is thought that the half bandwidth stays constant in an ideal system where no interaction at all occurs between PK and PA. However, the *FWHM* value of PK/PA polymer alloys is smaller than those of each element polymers (PA and PK). It revealed that the interaction occurred between PK and PA in the PK/PA polymer alloys. It appears that the *FWHM* values of the two peaks saturated at about $\phi_{PA} = 0.422$, i.e., for the K60A40 sample. This result suggests that combining PK and PA into an alloy increases the interaction between them. Presumably, this interaction is related to the phase separation structure between PK and PA and changes in the crystal structure of both phases. With regard to the former structure, Takahashi et al.[39] have found on the basis of SAXS and TEM observations that the polymer alloy consists of the lamellar network of PK and the nano-level phase separation structure of PK/PA. Nishioka et al.[40] and Asano et al.[41] used high resolution solid-state $^{13}$C-NMR to measure the relaxation time $T_1^H$ and $T_{1\rho}^H$ of wet and dry K60A40 polymer alloy samples and reported that from the standpoint of molecular chain kinematics, there was no interaction between PK and PA at a distance of 2–5 nm, but there was interaction between them at a distance of 20–50 nm. The latter structure is a subject for future study.

### Morphology of PK/PA polymer alloy

Figure 7(a) shows TEM images of K60A40 observed by low and high magnification. The deep and light color regions are presumably the PA-rich phase stained with phosphor tungstic acid and the hard-to-stain PK-rich phase, respectively. Network and particle patterns can be observed in these images. The network in particular displayed a lamella pattern. EELS mapping images of the same views as the TEM observations are shown in Figure 7(b). The white parts indicate the presence of N that

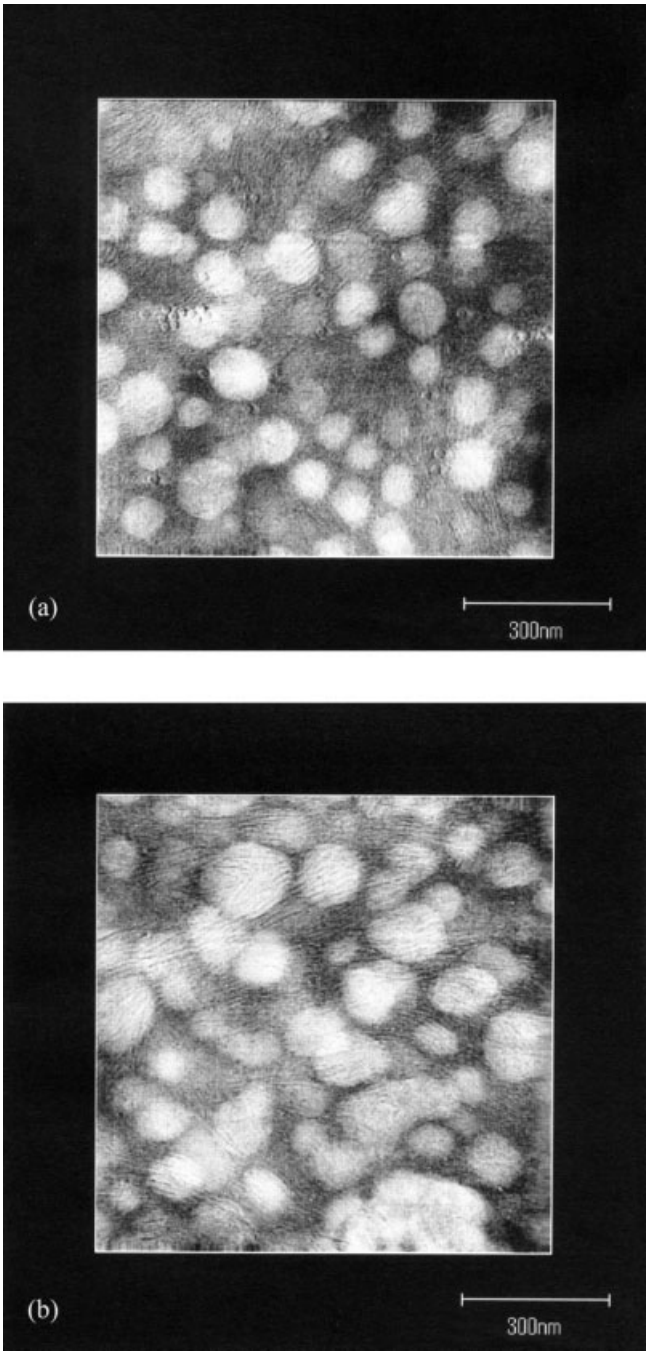


**Figure 8** 3D-TEM images of K90A10 and K80A20: (a) K90A10, (b) K80A20.

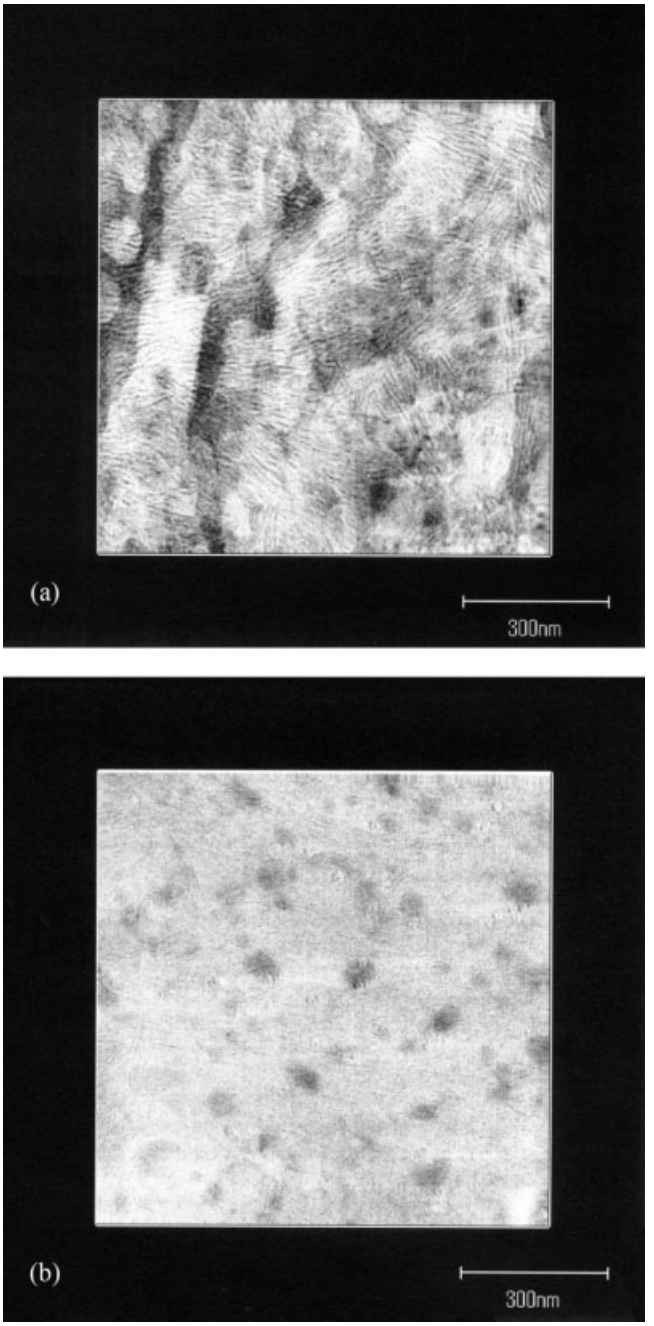


**Figure 9** 3D-TEM images of K60A40 and K10A90: (a) K60A40, (b) K10A90.

originated from PA. A comparison of Figure 7(a,b) reveals that N was noticeably scarce in the region of the lamella network. This result implies that the lamella network was formed in the PK-rich phase of K60A40.

A 3D-TEM was used in order to observe three-dimensional images of the lamella network at the nanometer level. Figure 8(a,b) is 3D-TEM image of K90A10 and K80A20, respectively. A lamella-filled spherical region of about 500 nm in size was observed in both samples. 3D-TEM images of K60A40 and K10A90 are shown in Figure 9(a,b), respectively. The spherical region was not observed in K60A40. The formation of a three-dimensional co-continuous structure consisting of the lamella network of the PK-rich phase and the PA-rich phase at the nanometer level was observed in this sample. The lamella network was also observed in K10A90. Considering the PK loading (10 mass %), it is inconceivable that the entire lamella network was composed of the PK-rich phase. Let us look carefully at K60A40 and K10A90. Takahashi et al.[39] reported that the lamella thickness (about 14 nm) of K60A40

was larger than that (about 8 nm) of K10A90. This suggests that the components of the lamella network differed between the two samples. The lamella thickness of K60A40 might correspond to that of PK, whereas the lamella thickness of K10A90 might represent that of PA. Additionally, the lamella network is discussed next with respect to the SAXS measurement results.

On the other hand, Smith et al.[42] reported that phase inversion occurs when the minority component becomes the continuous phase and the majority component is dispersed, and this phenomenon, which is generally observed under melt-shear conditions, normally depends on blend composition and the viscosities of the polymer components. According to Chuai et al.,[43] with increasing volume fraction of one of the phases, if a previously continuous phase becomes discontinuous (thus switching the role of "network" and "particles" in a polymer blend), the volume fraction at which the switching occurs is known as "phase inversion" point. Considering the aforementioned, it is thought that the alloys (i.e., K90A10 and K80A20) containing high PA loading, consist of one phase in the matrix of the second phase, more balanced compositions (i.e., K60A40) yield co-continuous structures at a phase inversion point, and the phase-inversed structure such as K10A90 formed over the point. This speculation is supported by the 3D-TEM observation results.

### Lamella network

Figure 10(a,b) shows the respective SAXS measurement results for the dry and wet PK/PA polymer alloys. The vertical and the horizontal axes indicate the X-ray diffraction strength and the scattering angle (2θ), respectively. For the dry K100 sample [Fig. 10(a)], a shoulder was observed at 2θ of about 0.8°. The K90A10 and K60A40 samples had a peak at this 2θ. The peak strength increased with an increase in PA loading from K90A10 to K60A40. A calculation of the long period ($d$) for 2θ = about 0.8° by using the Bragg equation [$\lambda = 2d \sin\theta$; $d$, long period (i.e., lamella thickness); λ, wavelength of X-rays; θ, scattered angle] yielded a value of approximately 13 nm. The peak strength decreased with an increase in PA loading from K70A30 to A100. In this loading region, the 2θ value at the peak gradually increased from about 0.8° with an increase in PA loading. An increase in 2θ means a decrease in $d$. The $d$ value of A100 was about 8 nm. These results suggest that PA loading promoted an increase in the lamella of the PK-rich phase in the region from K100 to K60A40. The amount of lamella decreased with an increase in PA loading in the region from K70A30 to A100. There was a pronounced difference in the amount of lamella especially between K10A90 and A100. The component of the lamella also changed from the PK-rich phase to the PA-rich phase in the region from K70A30 to A100. It is seen in Figure 10(b) that the wet polymer alloys had almost the same amount of lamella as the dry ones, though 2θ at the peak decreased a little with an increase in moisture absorption. For example, the $d$ value of the dry K60A40 sample was about 13 nm, whereas that of the wet K60A40 sample was about 14.5 nm. These results suggest that the amorphous regions between the crystal lamella, that is, the interlayer contain a small amount of PA and are swollen by moisture.

### Molecular motion of wet and dry polymer alloys

Figure 11 shows the solid-state high resolution NMR ($^{13}$C CP/MAS NMR) spectra of the dry and wet K60A40 samples at room temperature. The signal strength is shown along the vertical axis in relation to the chemical shift along the horizontal axis. The solid and dotted lines are the wet and dry samples,

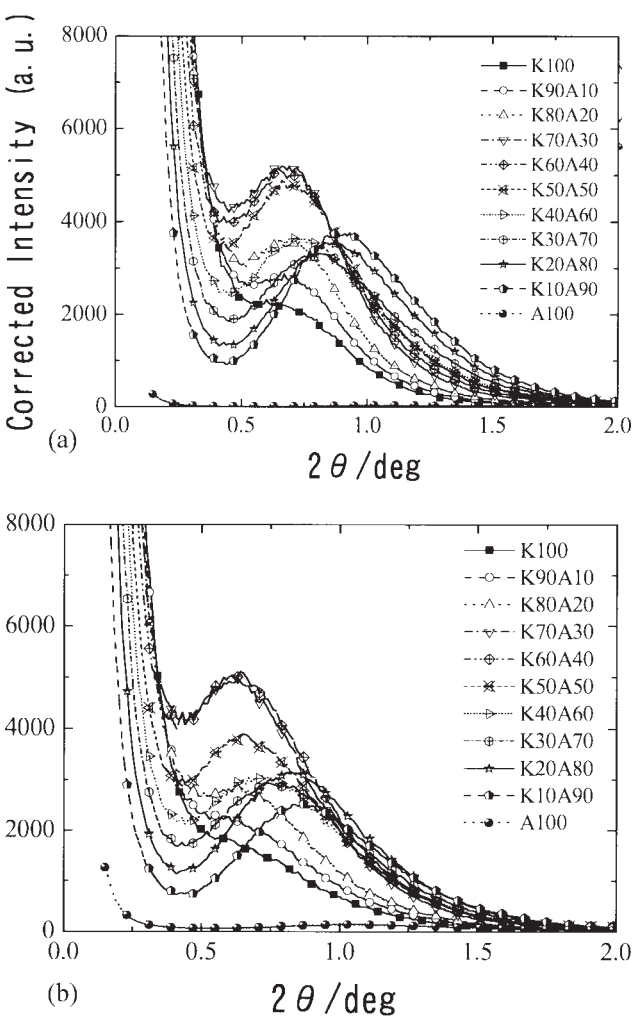


**Figure 10** SAXS measurement results for dry and wet PK/PA polymer alloys: (a) Dry samples, (b) wet samples.

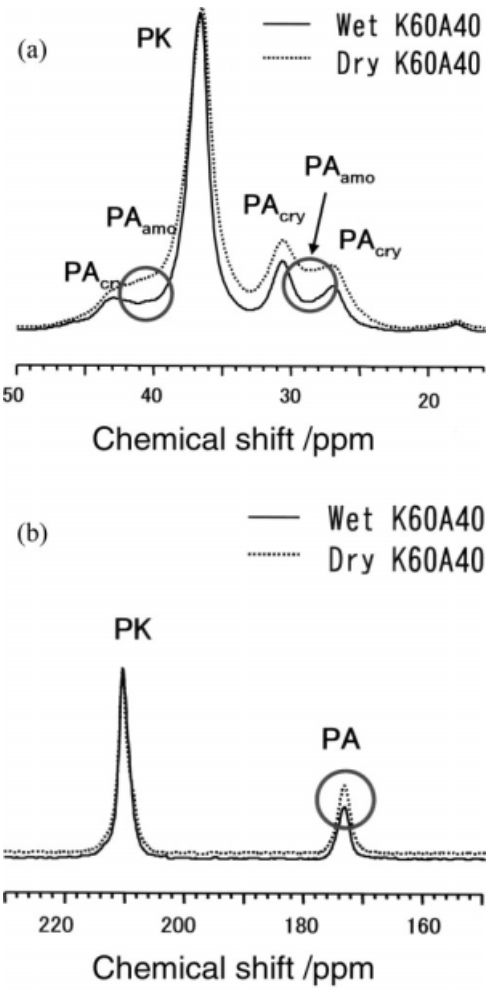


**Figure 11** $^{13}C$ CP/MAS NMR spectra of wet and dry K60A40 samples.

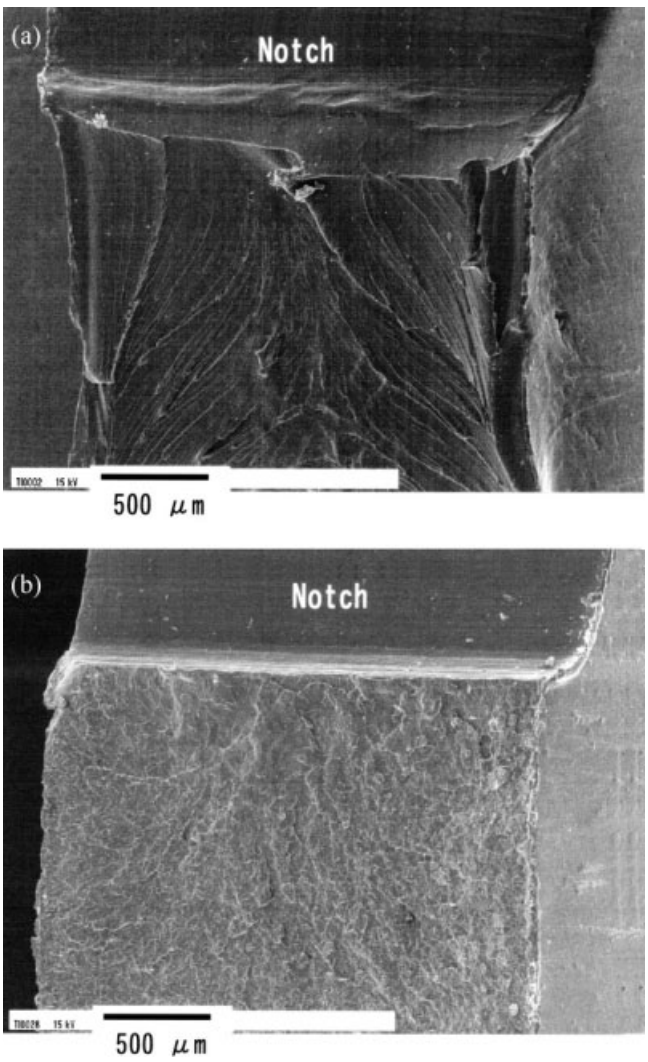


**Figure 12** Fracture surface images of wet (moisture-absorbed) and dry K60A40 samples: (a) Wet K60A40, (b) dry K60A40.

respectively. PK had only two signal peaks at 37 and 210 ppm, which were independent of moisture absorption. The signal peaks at *ca.* 27, 29, 31, 41, 43, and 170 ppm, which are attributed to total, crystal amorphous PA, are indicated as PA, $PA_{cry}$, and $PA_{amo}$ in this figure. It is known that the NMR signal strength decreases when molecular motion becomes higher than the NMR signal frequency. Notice that the PA and $PA_{amo}$ signal strength of the wet K60A60 sample was lower than that of the dry one. This implies that moisture absorption enhanced the motion of PA. Such higher molecular motion may follow quick stimulation such as that in impact testing, and may be able to absorb more impact energy.

### Quantitative and qualitative impact properties

#### Morphology of impact fracture surface

Figure 12(a,b) shows magnified views of the Charpy fracture surface near the fracture origin of wet and dry K60A40 samples, respectively. The notch is shown at the top of each fracture surface. The morphology of the wet sample [Fig. 12(a)] indicates shear yielding, which is typical of ductile fracture. In contrast, the dry sample has an angular fracture surface that is typical of brittle fracture. These results imply that absorption of moisture improved the ductility of this polymer alloy.

#### Load-displacement curves in Charpy impact test

Figure 13 shows the load-displacement curves obtained in Charpy impact tests conducted on wet K100, K60A40, and A100 samples. These curves show a conical pattern with a peak top, and the height of the peak tends to increase with increasing $MF_{PA}$. The load-displacement curve obtained from a Charpy impact test is diagrammed schematically in Figure 14. This load-displacement curve has been simplified to an asymmetric conical pattern. The

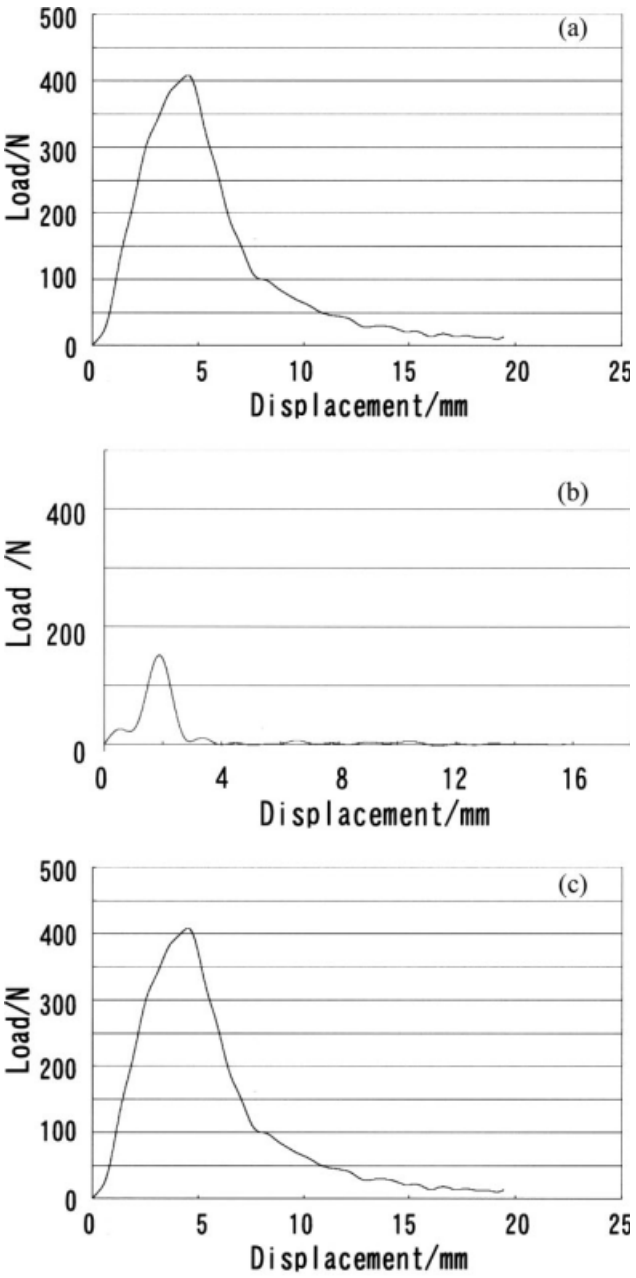


**Figure 13** Load-displacement curves obtained from Charpy impact testing for wet PK/PA polymer alloy: (a) Wet K100, (b) wet A100, and (c) wet K60A40.

maximum stress (*MS*) was calculated from the maximum load at a peak top of the load-displacement curve in Figure 14. The displacement at the *MS* was defined as the displacement ($D_{MS}$). The curve was divided into two portions at the peak top and the energy found for each area was defined as the energy of crack generation at the notch front ($E_1$) and the energy of crack propagation ($E_2$). The sum of the two values is the total impact absorption energy ($E_{total}$).

The *MS* and the $D_{MS}$ of the dry and wet polymer alloy samples as a function of the PA mass fraction

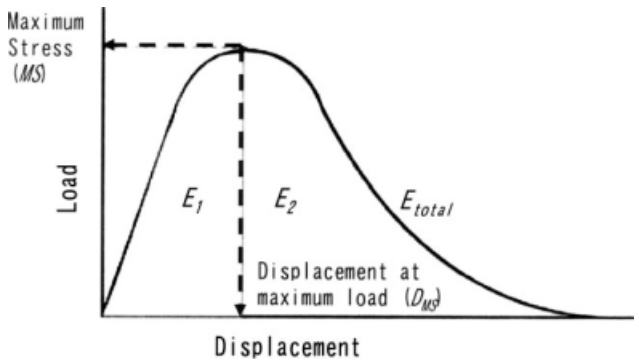


**Figure 14** Schematic diagram of load-displacement curve obtained from Charpy impact test. $E_1$, energy of crack generation at notch front; $E_2$, energy of crack propagation; $E_{total}$ ($= E_1 + E_2$), total impact absorption energy.

($MF_{PA}$) are shown in Figure 15(a,b), respectively. The dry and wet K60A40 samples displayed nearly the same *MS* values, but the wet sample showed larger $D_{MS}$ than the dry sample. These results indicate that $MF_{PA}$ did not change the mechanical strength of the polymer alloys appreciably, but it did increase their deformation markedly. This result supports the ductile fracture exhibited by the wet polymer alloy sample in Figure 12(a). With regard to the improved ductility of the PA phase due to moisture absorption, Nishioka et al.[40] and Asano et al.[41] investigated wet and dry K60A40 samples by $^{13}$C-NMR spectroscopy and found that the mobility of PA molecules was markedly higher in the wet samples than in the dry ones. This implies that moisture absorption enhances the mobility of PA molecule chains, making it easier for large deformation to occur.

The $E_{total}$, $E_1$, and $E_2$ values found for the wet and dry polymer alloy samples are shown in Figures 16 and 17, respectively. In the case of K70A30 and K60A40, the energy levels were higher for the wet samples than for the dry ones. The largest energy values are seen for the wet K60A40 sample. It is especially interesting that distinct increases in $E_2$ due to moisture absorption are seen in the order of K70A30 followed by K60A40, whereas the values of the other samples in both their wet and dry states were nearly the same. These results indicate that in a range of $MF_{PA} = 0.3$–$0.4$ (K70A30 and K60A40, PA volume fraction 0.320 and 0.422), the pronounced increase in $E_2$ due to moisture absorption, in addition to the increase in $E_1$, contributed to increasing $E_{total}$. Furthermore, taking into account the magnitude of the energy, $E_2$ contributed more to increasing $E_{total}$ than $E_1$ in this $MF_{PA}$ range. The wet K70A30 and K60A40 samples in particular showed a marked increase in deformation, which increased the energy of crack generation at the notch front ($E_1$). Moreover, the energy of crack propagation ($E_2$) of

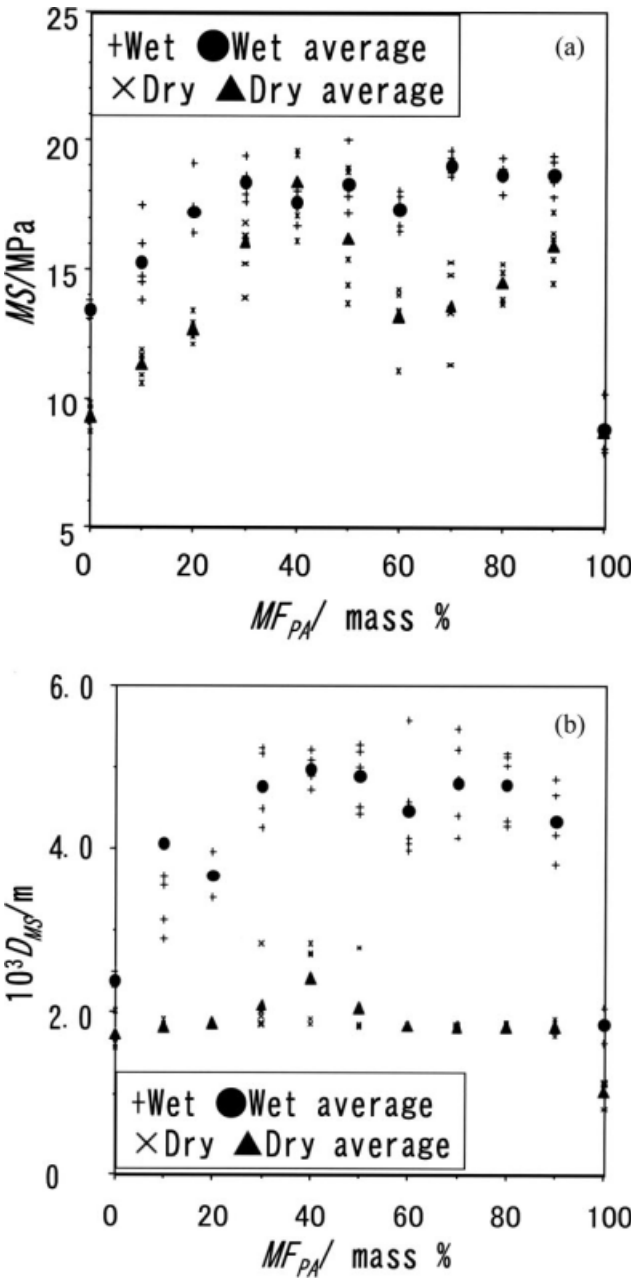


**Figure 15** Dependence of maximum stress (*MS*) and displacement ($D_{MS}$) at *MS* on PA mass fraction ($MF_{PA}$): (a) *MS*, (b) $D_{MS}$.

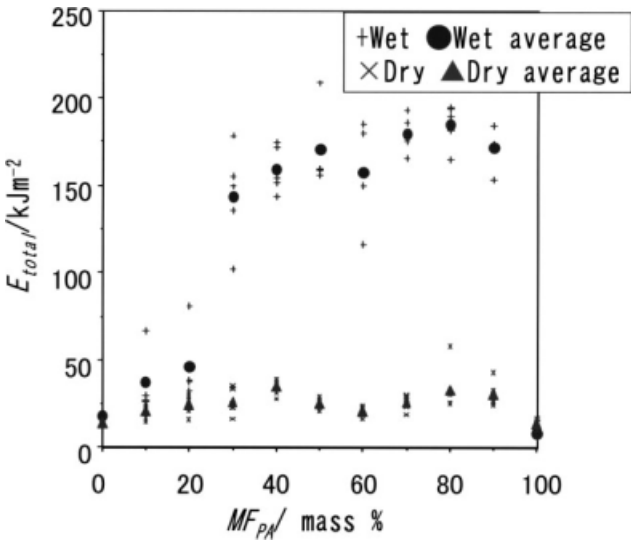


**Figure 16** Relationship total impact absorption energy ($E_{total}$) and PA mass fraction ($MF_{PA}$) of wet and dry samples.

these samples showed an even larger distinct increase for some reason, resulting in a noticeable increase in their $E_{total}$ values as well. For example, the $E_{total}$ value of PC is 10–80 kJ/m$^2$.[31,32] With regard to this particular increase in $E_2$, it is assumed that the PA phase became a stress concentrator following the large deformation of the test sample, causing crazes to form around it which promoted the absorption of energy.

On the other hand, if only the PA phase of the wet polymer alloy samples showed a marked increase in elongation and the PK phase was unable to follow that change, the test samples would fail at an early stage; thus, no increase in impact energy absorption could be expected. Accordingly, in order for the PK phase to be able to follow the change in elongation of the PA phase, it is necessary to consider the interface between the incompatible PK/PA phases. Inoue and Ougizawa[44] proposed that the size ($d_{ip}$) of the island phase in a system of two incompatible polymers is proportional to the interfacial tension ($\sigma$) between the two components. Broseta et al.[45] reported that $\sigma$ in such polymer systems is proportional to the interaction parameter between the components ($\chi$) and that $\chi$ is inversely proportional to the equilibrium interfacial thickness ($\lambda_{ip}$). These observations mean that $\lambda_{ip}$ increases as d decreases. In other words, in a polymer alloy composed of two incompatible constituent polymers, like the polymer alloy samples examined in this study, it can be inferred that the interfacial thickness of the two phases, i.e., the interaction between the phases, increases as the size of the island phase decreases.

## CONCLUSIONS

It has been reported that polymer alloys consisting of PK and PA 6 exhibit Izod impact strength equal to or greater 0.05–1 kJ/m of PC and that the absorption of moisture markedly increases their impact strength. The DSC thermograms of PK and PA show two distinguishable $T_g$ values corresponding to the respective neat polymers, whereas K60A40 has two $T_g$'s and they are located between the $T_g$ of PK and that of PA. Furthermore, the dependence of the intensity ratio and full width at half maximum (*FWHM*) of the Raman shift peak on the PA volume fraction was

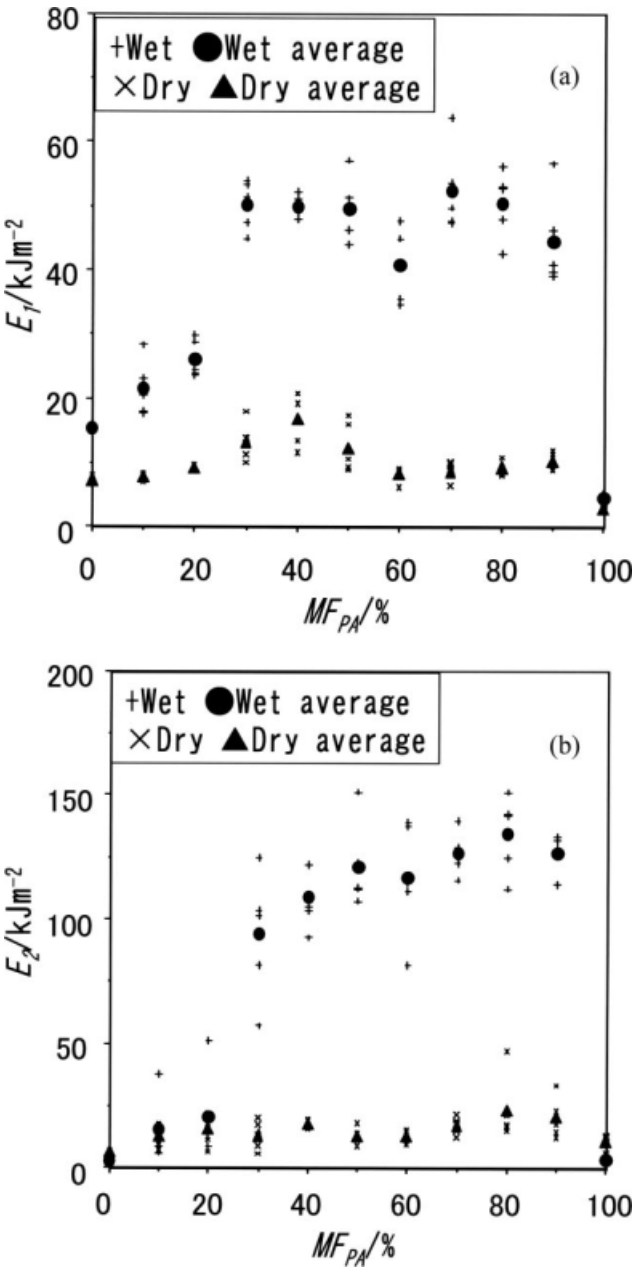


**Figure 17** Dependence of $E_1$ and $E_2$ on PA mass fraction ($MF_{PA}$) of wet and dry samples: (a) $E_1$, (b) $E_2$.

investigated. The results indicated that although PK and PA were in a physically mixed state in the polymer alloys without any chemical reactions (i.e., thermal decomposition and degradation, oxidation, hydrolysis, polymer reaction, copolymerization, etc.) occurring between them because that PK and PA are thermally and chemically stable under this mixing and molding conditions, whereas a microscopic interaction phase was formed between the PK and PA phases. The reason for the formation of the interaction phase consisting of both PK and PA is attributed to a decline in their surface tension due to the mixing of the two components at the nanometer level. Furthermore, we have investigated the micro phase separation structure of PK/PA alloys by using TEM, EELS, and 3D-TEM observations. It was found that the PK-rich phase and the PA-rich phase form an island-sea, a co-continuous, or a phase-inversed structure. Surprisingly, the three-dimensional lamella network structure extended into the PK-rich phase. SAXS measurements were performed to evaluate the lamella network structure. Moreover, the interaction and mobility of PK and PA molecular chains were investigated by using a solid-state high resolution NMR technique.

Instrumented Charpy impact tests were then conducted on wet (moisture-absorbed) and dry (dried) PK/PA polymer alloy samples. The wet impact test samples displayed a ductile fracture surface, whereas the dry impact test samples displayed a brittle fracture surface. The maximum load and maximum displacement were found from impact load-displacement curves obtained in the impact tests for the wet and dry polymer alloy samples. The maximum load (*MS*) was found to be nearly the same for both the wet and dry samples, but the wet samples showed a marked increase in the displacement ($D_{MS}$) at *MS* compared with their dry counterparts. It was inferred from these results that the increase in impact strength displayed by the wet samples originated from a marked increase in deformation due to moisture absorption.

An investigation was made of the total impact absorption energy ($E_{total}$), energy of crack generation at the notch front ($E_1$) and energy of crack propagation ($E_2$) of the polymer alloy test samples. While moisture absorption tended to increase $E_{total}$ in general, it was observed that polymer alloys (notably K60A40 and K70A40: The former was mixed with $\sim$ 60 mass % PK and 40 mass % PA, and the later was composed from 70 mass % PK and 30 mass % PA.) showed a distinct increase only in $E_2$ as a result of absorbing moisture. It is presumed that, after a test sample underwent large deformation, the PA phase became a stress collector, causing shear deformation exclusively around it that promoted energy absorption, which would explain the distinct increase observed in $E_2$. For the K60A40 and K70A30 polymer alloy samples, $E_2$ was more dominant than $E_1$ in increasing $E_{total}$. Furthermore, the reason why the PK phase was able to follow the elongation of the moisture-absorbed PA phase without fracturing is probably due to the presence of an interaction phase near the interface between the co-continuous nano layers. Strictly speaking, these nano layers are the amorphous regions between the crystal lamellae, that is, the interlayer. The interaction phase was formed in regions close to both the PA-rich and the PK-rich phase. These results imply that the phase separation structure and higher-order

structure are closely related to mechanical properties.

The authors thank Mr. Junzou Ootake at the Industrial Technology Center of Okayama Prefecture for his technical advice and Mr. Hidenori Sato, Mr. Daisuke Ishikawa, and Mr. Masaru Hashimoto at Nissan Arc, Ltd. for their cooperation with this study.

## References

1. Charlesworth, D. Mater Des 1981, 2, 149.
2. Waterman, N. A.; Neal, M. Mater Des 1981, 2, 250.
3. Edwards, K. L.; Davies, G. Mater Des 2006, 27, 172.
4. Li, Y.; Lin, Z.; Jiang, A.; Chen, G. Mater Design 2004, 25, 579.
5. Singh, R.; Mattoo, A.; Saigal, A. Mater Design 2006, 27, 955.
6. Wu, S. Polym Int 1992, 29, 229.
7. Michler, G. H. Acta Polym 1993, 44, 113.
8. Yamamoto, T.; Furukawa, H. Polymer 1995, 36, 2393.
9. Majumdar, B.; Keskula, E. J.; Paul, D. R. J Polym Sci 1997, 32, 2127.
10. Lombardo, B. S.; Keskkula, E.; Paul, D. R. J Appl Polym Sci 2003, 54, 1697.
11. Greco, R.; Sorrentino, A. Adv Polym Technol 2003, 13, 249.
12. Tan, Z. Y.; Xu, X. F.; Sun, S. L.; Zhou, Y. H.; Zhang, H. X.; Han, Y. Polym Eng Sci 2006, 46, 1476.
13. Tortorella, N.; Beaty, C. L. Polym Eng Sci 2008, 48, 2098.
14. Kuriyama, T. Polym Process 1999, 11, 273, (in Japanese).
15. Bucknall, C. B. Toughened Plastics; Applied Science Publishers, Ltd.: London, 1977.
16. Bucknall, C. B. In Polymer Blends; Paul, D. R., Bucknall, C. B., Eds.; Wiley: New York, 2000.
17. Narisawa, I. Polym Eng Sci 1987, 27, 42.
18. Fu, S.; Shen, J. J Appl Polym Sci 1993, 49, 673.
19. Nagata, K.; Hikasa, S.; Sakaki, D.; Kobayashi, J.; Miyahara, K.; Izumi, T.; Toyohara, M.; Kato, A.; Nakamura, Y. Adhesion 2007, 43, 343, (in Japanese).
20. Okamoto, K.; Miyagi, H.; Kakugo, M.; Uno, T. Sumitomo Chemical Annual Report 1992, 1992, 42, (in Japanese).
21. Cleslinski, R. C.; Silvis, H. C.; Murray, D. J. Polymer 1995, 36, 1827.
22. Chakrabarty, D.; Das, B.; Roy, S. J Appl Polym Sci 1998, 67, 1051.
23. Pecorini, T. J.; Calvert, D. ACS Symp Ser Am Chem Soc 2000, 759, 141.
24. Hobbs, S. Y.; Dekkers, M. E. J.; Watkins, V. H. Polym Bull 1987, 17, 341.
25. Kim, G.-M.; Michler, G. H. Polymer 1998, 39, 5689.
26. Bucknall, C. B.; Gilbert, A. H. Polymer 1989, 30, 213.
27. Phan, T. T. M.; Denicola, A. J.; Schadler, L. S. J Appl Polym Sci 1998, 68, 1451.
28. Chen, H.; Yang, B.; Zhang, H. J Appl Polym Sci 2000, 77, 928.
29. Nagata, K.; Hikasa, S.; Iwabuki, H.; Nishioka, M.; Kato, A.; Sawabe, H.; Takahashi, Y.; Sato, H.; Asano, A. Polym Prepr 2007, 56, 2D15, CD-ROM, (in Japanese).
30. Available at: http://www.rostravernatherm.com/images/pdf/polycarbonate_data.pdf.
31. Available at: http://www.idemitsu-chemicals.de/16-0-polycarbonate-tarflon.html.
32. Kato, A.; Ikeda, Y.; Kasahara, Y.; Shimanuki, J.; Suda, T.; Hasegawa, T.; Sawabe, H.; Kohjiya, S. J Opt Soc Am B 2008, 25, 1602.
33. Kohjiya, S.; Kato, A.; Ikeda, Y. Prog Polym Sci 2008, 33, 979.
34. The IMOD home page, Boulder Lab for 3D Electron Microscopy of Cells. Available at: http://bio3d.colorad.edu/imod/index.html.
35. TGS-MAXNET-amira documentation. Available at: http://www.maxnt.co.jp/support/amira_doc.
36. Feng, J.; Chan, C. M. Polymer 1997, 38, 6371.
37. Sommazzi, A.; Garbassi, F. Prog Polym Sci 1547, 197, 22.
38. Zhang, X; Loo, L. S. Polymer 2009, 50, 2643.
39. Takahashi, Y.; Nishioka, M.; Sawabe, H.; Sato, H.; Kato, A.; Nagata, K.; Iwabuki, H.; Hikasa, S.; Asano, A. Koubunshi Ronbunshu 2009, 66, 577.
40. Nishioka, M.; Takahshi, Y.; Kato, A.; Sawabe, H.; Sato, H.; Nagata, K.; Hikasa, S.; Iwabuki, H.; Asano, A. Koubunshi Ronbunshu, 2009, 66, 570.
41. Asano, A.; Nishioka, M.; Takahshi, Y.; Kato, A.; Hikasa, S.; Iwabuki, H.; Nagat, K.; Sato, H.; Hasegawa, T.; Sawabe, H.; Arao, M.; Suda, T.; Mukai, M.; Ishikawa, D.; Izumi. T. Macromolecules 2009, 42, 9506.
42. Smith, A. P.; Ade, H.; Smith, S. D.; Koch, C. C.; Spontak, R. J. Macromolecules 2001, 34, 1536.
43. Chuai, C. Z.; Almdal, K.; Lyngaae-Jørgensen, J. Polymer 2003, 44, 481.
44. Inoue, T.; Ougizawa, T. New Polymer Experimentology 1, Fundamentals of Polymer Experiments and Analysis of Molecular Characteristics. Society of Polymer Science; Kyoritsu Shuppan: Tokyo, 1995 (in Japanese).
45. Broseta, D.; Fredrickson, G. H.; Helfand, E.; Leiber, L. Macromolecules 1990, 23, 132.